Hindawi
Wireless Communications and Mobile Computing
Volume 2022, Article ID 8431967, 11 pages
https://doi.org/10.1155/2022/8431967

Research Article

Spectrum Sensing of Noncooperative Beam Signals

Xieda Song, Jinghua Li, Jiteng Liu, Yan Li, and Guoru Ding

Army Engineering University of PLA, China

Correspondence should be addressed to Jinghua Li; chinghwali@126.com

Received 10 April 2022; Revised 13 June 2022; Accepted 16 June 2022; Published 30 July 2022

Academic Editor: Mingqian Liu

In this paper, we investigate the issue of spectrum sensing of noncooperative beam signals that are emitted by a multiantenna transmitter. When the sampling period of the sensing node includes the whole process of beam scanning, that is, spectrum sensing is performed in an ideal situation, we use the traditional energy detection algorithm for spectrum sensing and get good results; for multiantenna beam scanning spectrum sensing in nonideal situation, the performance of traditional energy detection algorithm is seriously degraded. To deal with this problem, a sensing period selection (SPS) algorithm is proposed. The simulation results show that the proposed algorithm can effectively improve the performance of spectrum sensing in the multiantenna array beam scanning scenario.

1. Introduction

With the rapid development of wireless communication technology, the spectrum resource demand is also increasing [1]. The ever-increasing demand for spectrum has led to a shortage of available spectrum resources [2]. Spectrum sensing, based on various signal detection approaches, is one key enabling technology for dynamic spectrum sharing [3]. Traditional spectrum sensing mainly detects omnidirectional signals, which include energy detection [4] matched filter detection [5], and cyclostationary detection [6]. As the 5G cellular communication technology emerges, spatial domain signal generated by beamforming technology provides more available bandwidth for people's daily spectrum needs, while meeting the ever-increasing transmission rate and throughput requirements [7, 8]. At the same time, the new generation of spectrum sensing technology has also changed from the detection of omnidirectional signals to the detection of directional signals, that is, spectrum sensing of beam signals. The beamforming technology uses complex digital signal processing technology to convert the regular excitation signal into the corresponding amplitude and phase of each beam by designing the antenna array to generate a high-gain directional beam [9]. Beamforming technology can not only effectively make up for the shortcoming of beam signal's rapid loss in spatial transmission but also exploit spectrum resources from the spatial angle dimension [10]. At present, the detection of spectral holes in the spatial angle dimension, that is, spectrum beam sensing technology, has become a new research trend [11].

In spectrum sensing, it is necessary not only to sense the status of spectrum resources by primary users but also to provide spatial angle information in the spectrum. In general, the end of spatial spectrum sensing is divided into two stages: detection and positioning [12]. The research of these two stages is generally independent of each other. In the detection stage of spatial spectrum sensing, the main purpose is to detect whether the primary user exists. In [13], the authors propose a spatial detection algorithm, using techniques such as interference alignment to explore spatial spectrum resources and improve detection performance; the work in [14] uses beamforming to sectorize the space and proposes a spatial spectrum sensing algorithm based on sector segmentation, which not only improves the detection performance but also provides information about spare sectors in space. In addition, direction-of-arrival (DOA) estimation is required in the positioning stage of spatial spectrum sensing. The multiple signal classification (MUSIC) algorithm is the most representative algorithm in the positioning stage of spatial spectrum sensing [15–17]. The work in [18] proposes combined detection and positioning algorithms, where the authors first use the traditional detection algorithm to perform

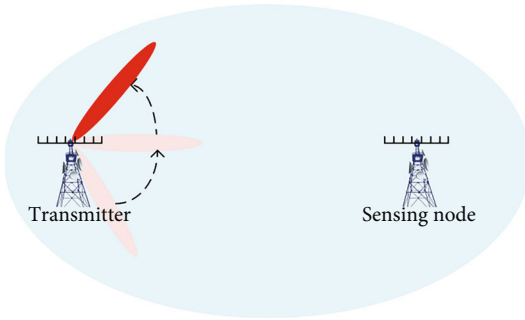

Figure 1: System model.

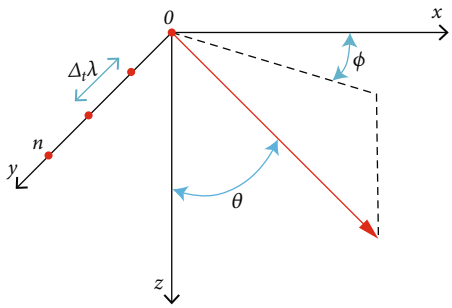

Figure 2: The deployment of antenna elements in linear array pattern.

spectrum sensing, then obtain the spatial information of spectrum holes through the angle-of-arrival (AOA) estimation algorithm to realize the function of spatial spectrum sensing.

This paper mainly studies the detection stage of spatial spectrum sensing in beam scanning scene. Specifically, this paper mainly studies spectrum sensing in multiantenna beam scanning scenarios, which is essentially spectrum sensing of beam signals. At this stage, there have been many papers on the spectrum sensing of multiantenna beamforming. The work in [19] proposes for multiantenna CR sensors a class of spectrum sensing methods, named the generalized likelihood ratio test (GLRT), that require no information about the primary users or the channels from the primary to the secondary users. The proposed methods utilize the eigenvalues of the sample covariance matrix of the received signal vector from multiple antennas and derive two new algorithms for spectrum sensing under different assumptions on the availability of the white noise power value at the CR receiver. The work in [20] designs a uniform circular array which uses a NC-α-MTG-MUSIC algorithm to sense the arrival signal. The NC-α-MTG-MUSIC includes an α-MTG algorithm to detect whether the primary signals exist and a MUSIC algorithm to estimate its DOA.

When a beamforming signal is sent to the receiver through the antenna array, the receiver's location information needs to be known. In other words, the beamforming direction needs to be determined. When the transmitter does not know the receiver's location, it generally determines the receiver's position information by beam scanning [21, 22], which provides an opportunity for sensing of noncooperative beam signals. There is no prior knowledge of beamforming arrays that can be obtained for noncooperative parties, which makes existing methods of spectrum sensing inapplicable. In this paper, a spectrum sensing method based on energy detection is proposed for the noncooperative beam scanning scenario. Since the noncooperative sensing party does not know any prior knowledge of the scanned signal, the energy detection method is the most effective spectrum sensing method in this scenario. Specifically, the main contributions of this paper are summarized as follows.

(1) Formulate a system model where the sensing node detects the presence of a beam scanning signal emitted by a noncooperative transmitter

(2) Derive the closed form expressions of the detection probability and the false alarm probability in beam scanning scenario

(3) Design an algorithm to improve spectrum sensing performance in nonideal situation of the beam scanning scenario by selecting the appropriate sensing time period

(4) Present in-depth simulation results which demonstrate the effectiveness of the proposed algorithm

The rest of the paper is organized as follows: Section 2 describes the system model, where we model the beam-scanning signal in the transmitter and the received signal in the receiver. Section 3 performs performance analysis of energy detection in beam scanning scenarios. In Section 4, a SPS algorithm is designed for spectrum sensing in nonideal situation. Section 5 presents the simulation results, including spectrum sensing results under ideal situation, spectrum sensing results under nonideal situation, and spectrum sensing results in nonideal situation after adding the proposed SPS algorithm. Section 6 concludes this paper.

2. Signal Model

In this paper, we consider a spectrum sensing system model as shown in Figure 1, which has a transmitter with a linear array to emit beam signals and a multiantenna sensing node to detect the presence of the beam signals. The transmitter is composed of a linear array of n_t antennas, which can generate a 0-180° scanning beam. The sensing node is located in the positive 90° direction of the beam generated by the noncooperative transmitter, where the beam starts to scan from 0°. Scanning beams ranging from 0° to 180° are generated by changing the phase of each transmit antenna. During the beam scanning process, the beam signal will cover the area where the sensing node is located. The sensing node is composed of a linear array composed of n_r antennas.

2.1. Transmitting Model. The transmitter consists of linear array antennas, and the number of antennas is n_t for a transmission channel from a transmitter to a sensing node. As shown in Figure 2, the azimuth and elevation angles are denoted by ϕ and θ, respectively, which obeys $\phi \in (-\pi, \pi]$ and $\theta \in (-\pi/2, \pi/2]$. Supposing that the path attenuation is the same for all antennas, the ith antenna transmit signal

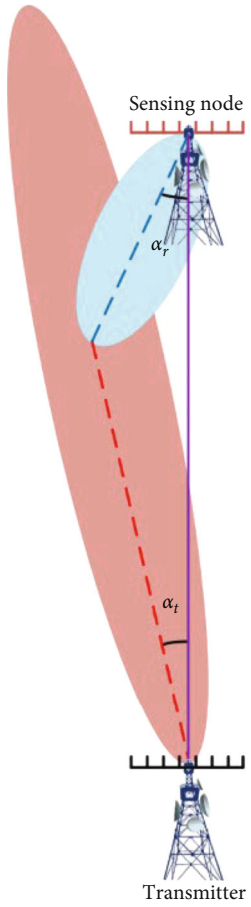

Figure 3: The beamforming gain with directional transmission and directional sensing node.

can be expressed as

$$y_i = Ae^{jd2\pi/\lambda}, \tag{1}$$

where A is the transmit power and d is the distance of signal propagation. λ is the carrier wavelength, and $\lambda = f/c$, where f is the carrier frequency and c is the speed of light. The distance between the two antennas is $\Delta_t\lambda$, the distance from the first antenna (the antenna that is closest to the receiver) to the sensing node is $d_1 = d_0$, the distance from the second antenna to the sensing node is $d_2 = d_0 + \Delta_t\lambda \sin\theta \cos\phi$, and the distance from the nth antenna to the sensing node is $d_n = d_0 + (n-1)\Delta_t\lambda \sin\theta \cos\phi$. Therefore, the beamforming vector can be expressed as

$$\mathbf{w_t} = \begin{bmatrix} 1 \\ \exp\left(j2\pi\Delta_t \sin\theta \cos\phi\right) \\ \exp\left(j2\pi 2\Delta_t \sin\theta \cos\phi\right) \\ \vdots \\ \exp\left(j2\pi(n_t-1)\Delta_t \sin\theta \cos\phi\right) \end{bmatrix}. \tag{2}$$

The channel vector can be obtained by

$$H = \exp\left(\frac{j2\pi d_0 \sin\theta \cos\phi}{\lambda}\right). \tag{3}$$

2.2. Sensing Model. The sensing node consists of a linear array of n_r antennas. When receiving the signal, the sensing node selects a direction to receive the signal. The sensing node is designed as a linear array to receive beam signals directionally. If the approximate direction of the transmit beam is known, interference from signals from other directions can be effectively reduced. The hypothesis is expressed by hyperparameters H_1 that the beam signal exists, and the absence of the beam signal is expressed by hyperparameters H_0 [23]. The received signal can be expressed as

$$y(n) = \begin{cases} \varepsilon(n), & H_0, \\ \mathbf{w_r^H H w_t} x(n) + \varepsilon(n), & H_1, \end{cases} \tag{4}$$

where $\mathbf{w_r}$ and $\mathbf{w_t}$ are the beamforming vector of the receiving beam and the beamforming vector of the transmitting beam, respectively. $\varepsilon(n)$ is additive noise following the zero mean additive white Gaussian noise (AWGN) distribution with variance δ_w^2. $x(n)$ is the symbol of the transmitted signal, denoted as $x_i(n) i = 1, 2, \cdots, n_t$, which is the output of the ith antenna, where n_t is the number of antennas. We define $|\mathbf{w_r^H H w_t}|^2$ as the beam alignment gain of the antenna G [23]:

$$G = G_r h G_t, \tag{5}$$

where G_r, G_t, and h denote the receive gain, transmit gain, and the channel gain, respectively, and their values depend on whether the beam is aligned. Here, we use the typical sector antenna model [24] expressing them as a function of the alignment angle:

$$G_n(\alpha) = \begin{cases} g_1 = \dfrac{2\pi - (2\pi - \varphi)g_2}{\varphi}, & \text{if } |\alpha_n| \le \dfrac{\varphi}{2}, \\ g_2, & \text{else}, \end{cases} \tag{6}$$

where n can be r or t. As shown in Figure 3, α_r and α_t represent the angle between the directional receiving beam and the optimal beam and the angle between the transmitting beam and the optimal transmitting beam, respectively. g_1 is the main beam gain, and g_2 is the sidelobe gain, which satisfies $0 \le g_1 \le 1 \le g_2$. φ is the bandwidth [25] of the beam in gain mode, which can be approximately expressed as

$$\varphi \approx 50.8 \frac{\lambda}{Nd \cos\beta}, \tag{7}$$

where β represents the angle between the beam pointing and the normal direction of the array.

3. Spectrum Sensing of Beam Signals

For noncooperative beam signals, the energy detection algorithm [26] can detect beam signals without prior information. The energy value of the received beam signal at the sensing node within a certain period of time is compared with a preset threshold, and if the received signal is higher than the threshold, it is determined that the beam signal exists [27].

Assuming that the channel is AWGN channel, the angular velocity of the transmitter to transmit the scanning beam is fixed. Note that x and ε both obey a Gaussian distribution. Therefore, we can conclude that the distribution of the received signal from formula (4) is

$$y(n) \sim \begin{cases} N\left(0, \delta_w^2\right) & H_0, \\ N\left(0, \delta_w^2 + G\delta_s^2\right) & H_1, \end{cases} \tag{8}$$

where G is the beam alignment gain; then, energy detection is used as a method for spectrum sensing. Let τ be the available sensing time and K be the number of samples (K is the maximum integer not greater than τf_s. For notation simplicity, we assume $K = \tau f_s$). The test statistic for energy detector is given by

$$\Lambda = \frac{1}{K} \sum_{n=1}^{K} |y(n)|^2, \tag{9}$$

where Λ, a random variable, is the energy detection statistic.

One key performance metric for energy detection is detection probability, which defines the probability that the detector detects the presence of a signal in H_1, which can be expressed as [28]

$$P_d = P(\Lambda > T | H_1). \tag{10}$$

Then, $p_1(x)$ is assumed to be expressed as the probability density function (PDF) of the energy detection statistic. Then, one key performance metric, named detection probability, can be further expressed as

$$P_d = \int_T^{\infty} p_1(x) dx. \tag{11}$$

Using central limit theorem (CLT), detection probability P_d can be given by

$$P_d = Q\left(\frac{T - \left(N\left(\delta_w^2 + G\delta_s^2\right)\right)}{\sqrt{(2/K)}\left(\delta_w^2 + G\delta_s^2\right)}\right), \tag{12}$$

where $Q(\cdot)$ is the complementary distribution function of the standard Gaussian,

$$Q(X) = \frac{1}{\sqrt{2\pi}} \int_x^{+\infty} e^{-t^2/2} dt. \tag{13}$$

Then, the missed detection probability can be expressed as

$$P_m = 1 - P_d. \tag{14}$$

Another key performance metric for energy detection is false alarm probability, which defines the probability that the detector detects the presence of a signal in H_0, which can be expressed as [28]

$$P_f = P(\Lambda > T | H_0). \tag{15}$$

Suppose $p_0(x)$ is represented as the PDF of the energy detection statistic Λ. Then, the probability of false warning can be given by

$$P_f = \int_T^{\infty} p_0(x) dx. \tag{16}$$

Using central limit theorem (CLT), false alarm probability P_f can be given by

$$P_f = Q\left(\frac{T - \delta_w^2}{\sqrt{2/K}\delta_w^2}\right). \tag{17}$$

4. Algorithm Design

In Section 3, we provide theoretical derivations for the performances of spectrum sensing in multiantenna beam scanning scenarios. As shown in Figure 4, the beam signal is scanned from 180° to 0°. The curves of different colors in Figure 4 represent the direction in which the transmitter emits the beam signal at different times, respectively. These performances can only be achieved under the ideal situation that the whole process of beam scanning is sampled by sensing nodes, and the sensing period is equal to the beam scanning period. In the actual situation, the process of beam scanning may not be completely sampled. Because the transmitter and the sensing node are noncooperative, it is difficult to set the sensing period to be the same as the beam scanning period. Therefore, for such a nonideal situation, we pay more attention to the sampling data of main lobe passing through the sensing node, where the time period is in t_s, as shown in Figure 4. We first assume that the sensing period t_s is the same as the time t_b for multiantenna beam scanning scenarios. In the spectrum sensing of beam scanning scenarios, we are more concerned about the energy detection statistics of the beam signal covering the sensing node, that is, the signal energy data in t_s time in Figure 4. If more data in the t_s can be sampled in the sensing cycle of the sensing node, the result of spectrum sensing will be greatly improved. Therefore, we propose an SPS algorithm to optimize the sensing results.

When the beam pattern covers the sensing node, the sensing node can detect a larger signal energy. Our goal is to collect the time period that the beam covers to the sensing node within the sensing period as much as possible. Therefore, the sensing performance will be greatly improved when the sensing node can collect more sampled data in the red area for spectrum sensing. In Figure 5, the transmitter starts

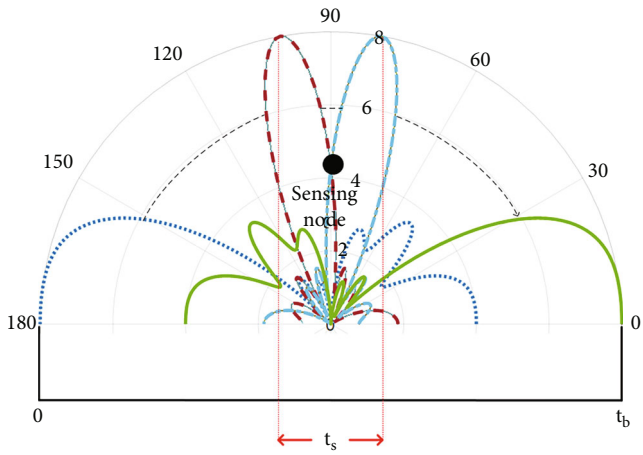

Figure 4: Important data sampling areas for spectrum sensing based on beam scanning.

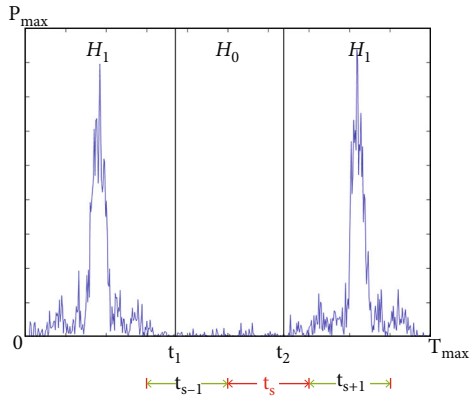

Figure 5: Signal energy data received by sensing node.

the first beam scanning at the time 0-t_1, the transmitter is off at the time t_1-t_2, and the transmitter starts the second round of beam scanning at the time t_2-T_{max}. We assume that the presence of the beam scanning signal in the t_s time period is to be sensed. The horizontal axis in the figure is a random period with a total time of T_{max}, including two complete beam scans of the transmitter. The longitudinal axis is the signal energy of the sensing node. In fact, during the t_s time period, the transmitter has started beam scanning. However, the time period in which the beam pattern covers the sensing node is not included in the t_s time, so the sensing node will mistakenly judge that the beam scanning signal does not exist. If we observe the sensing results in the t_{s+1} time period later, the sensing node will perceive the scanning signal correctly. Based on this idea, we design an SPS algorithm to improve the spectrum sensing performance in the case of nonideal beam scanning.

In nonideal situation, no matter when the sensing period starts, two sensing periods must contain the time for the whole beam scanning round. Suppose that the part of the process of beam scanning is sensed by the kth sensing cycle, then we need to compare the energy detection statistic Λ_k of the kth sensing cycle with the energy detection statistic Λ_{k-1} of the previous sensing cycle and the energy detection statistic Λ_{k+1} of the next sensing cycle. Comparing the largest energy detection statistic to a threshold, then the presence or absence of a beam scan signal will be given. The reason is we do not know whether the beam scanning process in the kth sensing period is the first half or the second half in t_b. Taking these three sensing periods can ensure that the whole beam scanning process is included. We can simplify this process by comparing these three energy detection statistics with the threshold. If they are all less than the threshold, the sensing result is H_0, otherwise, the perception result is H_1. When $t_s = t_b$, the algorithm is as follows.

When $t_s > t_b$, the whole beam scanning time must be included within 2 sensing cycles. Therefore, we can also use Algorithm 1 to optimize spectrum sensing. In this case, we cannot make the sensing time t_s too long. Because if the sensing time is too long, it will cause the sensing node to collect too many noise signals, which will eventually make the sensing result worse.

Then, we consider the case where the sensing period is smaller than the beam scanning period. We solve this problem by designing Algorithm 2. When $t_s < t_b$, we need to find an ideal integer i where $(i-1)t_s < t_b$ and $it_s > t_b$. Therefore, it can be ensured that the whole process of beam scanning must be included in i sensing cycles. Subsequently, similar to subsection C, the energy detection statistics for the first i and last i sensing cycles are compared to the threshold, respectively ($(2i+1)$ sensing cycles in total). If they are all less than the threshold, the sensing result is H_0, otherwise, the sensing result is H_1. In particular, we do not have to determine the ideal integer i. We need to estimate a small i where $it_s > t_b$, and we will get good results. The algorithm is as follows:

In addition, the case of $t_s \geq t_b$ can be regarded as the case of $i = 1$.

5. Simulation Results

In this section, we discuss the performance of the proposed energy detection method in the beam scanning scenario through numerical simulations and verify the theoretical analysis. Simulation results were investigated by running 10,000 iterations of Monte Carlo testing. The theoretical results are calculated using formulas (12) and (17). Considering the energy detection situation in the actual scene, we discussed the full process of beam scanning that sensing nodes are sampled and only part of the beam scan is sampled. The parameters in our simulation are shown in Table 1.

5.1. Sensing Results in Ideal Situation. In this subsection, we discuss the ideal case where the whole process of beam scanning is sampled by the sensing node and the sensing period t_s is the same as the time for one round of beam scanning t_b. In this case, the hyperparameter H_0 is defined as the transmitter which is not powered on during the sampling period of the sensing node; the hyperparameter H_1 is defined as the whole process of beam scanning which is sampled by the sensing node during the sensing period.

Input: threshold T, Energy detection statistics of the $(k-1)$-th sensing cycle Λ_{k-1}, Energy detection statistics of the k-th sensing cycle Λ_k, Energy detection statistics of the $(k+1)$-th sensing cycle Λ_{k+1}.
Output:H
1: If $\Lambda_{i-1} < T$ & $\Lambda_i < T$ & $\Lambda_{i+1} < T$
2: $H \leftarrow H_0$
3: Else
4: $H \leftarrow H_1$
5: End if

Algorithm 1: Equal period selection (EPS).

Input: threshold T, i, Energy detection statistics $\Lambda_{k-i} \ldots \Lambda_{k-1}$, Λ_k, $\Lambda_{k+1} \ldots \Lambda_{k+i}$.
Output:H
1: If $\Lambda_{k-i} < T$ & $\Lambda_{k-i+1} < T$ &…& $\Lambda_{k+i} < T$
2: $H \leftarrow H_0$
3: Else
4: $H \leftarrow H_1$
5: End if

Algorithm 2: Sensing period selection (SPS).

Table 1: Key simulation parameters.

Parameter	Value
Carrier frequency	$f_s = 28$ GHz
Maximum transmit power	$P_{\max} = 10$ W
Number of antennas	$n = 8$
Distance between antennas	$d_a = \lambda/2$
Distance between antenna array and receiver	$d = 10 \sim 50$ m
Loss	$\alpha = 2$

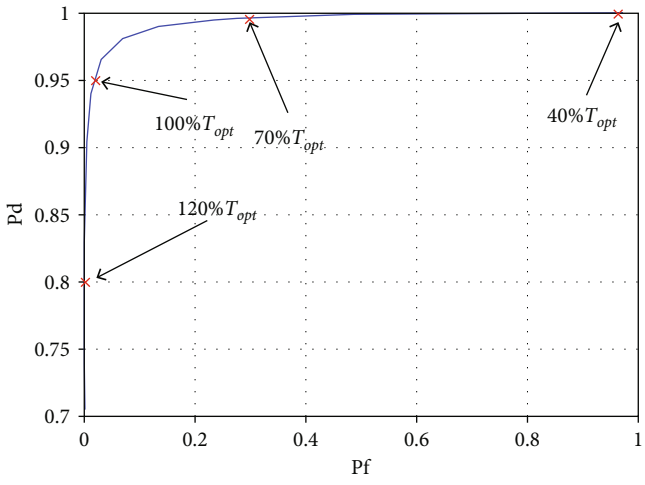

Figure 6: ROC curves of P_d and P_f in ideal situation.

Figure 6 shows the ROC curves of P_d and P_f at different thresholds. Setting different thresholds has a great impact on perceptual performance. If the threshold is set too large, some beam signals with weak energy may not be detected, resulting in reduced detection probability. If the threshold is set too small, the energy of some noise may have exceeded the threshold, resulting in an increase in the probability of false alarm probability. The threshold ranges from 40% T_{opt} with a step size of 5% to 100% T_{opt} which is defined as obtaining the optimum value of T_{opt} which results in target $P_d \geq 0.95$ while minimizing P_f.

Figure 7 shows the comparison between theoretical and simulated probabilities for P_d in different transmit powers with setting the threshold to make P_f as 0.01. It is seen that the probability of detection increases with the increase of the number of samples. As the transmit power increases, the signal power at each moment in the beam scanning process increases, too. It leads to an increase in SNR at any time in beam scanning process. So P_d will gradually become larger.

In Figure 8, we discussed the relationship between P_d and the change in the distance from the sensing node to the transmitter when the threshold is set to make P_f as 0.01. Figure 8 also shows the theoretical and simulated results of P_d. Obviously, when the distance increases to a certain extent, it decreases rapidly as the distance continues to increase. This is because the beam power in the wireless channel attenuates rapidly as the distance increases, and after the attenuation reaches a certain level, the power of beam signal is lower than noise.

5.2. Sensing Results in Nonideal Situation. In this subsection, we discuss a more realistic case where the part of the beam scanning process is sampled by the sensing nodes. In this case, the hyperparameter H_0 is defined as the transmitter which is not powered on during the sampling period of the sensing node; the hyperparameter H_1 is defined as the sampling period of the sensing node which contains the part of the beam scanning process.

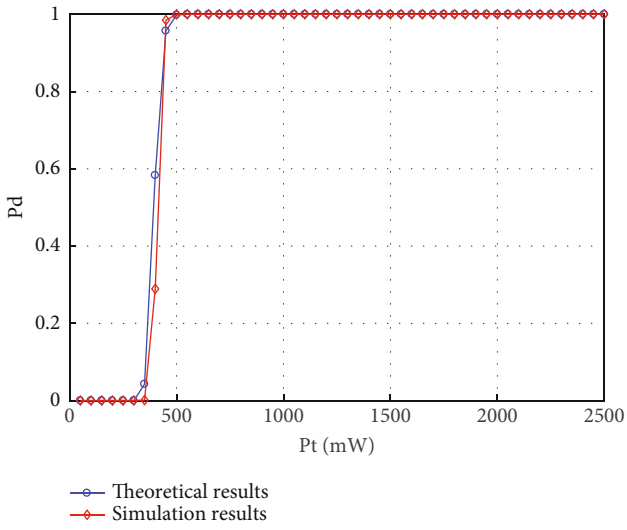

Figure 7: P_d as a function of power in ideal situation

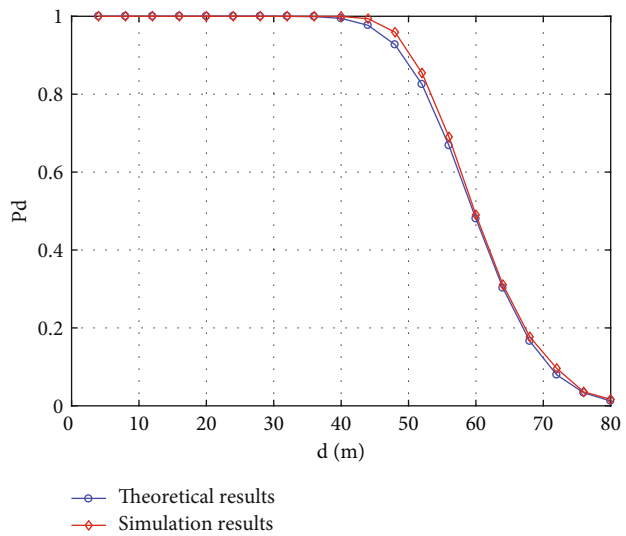

Figure 8: P_d as a function of distance in ideal situation.

The green curve in Figure 9 shows the ROC of P_d and P_f at different thresholds. Since the sensing node does not sample the whole process of beam scanning, the calculation results of equations (11) and (15) cannot be used to approximate the calculation results. In this case, simulation results were investigated by running 10,000 iterations of Monte Carlo testing.Comparing with Figure 6, the performance of the sampling partial scan process is significantly lower than that of the sampling full scan process.

The green curve in Figure 10 shows the variation of P_d in different transmit powers with setting the threshold to make P_f as 0.1. We find that with transmit power increased, P_d increases gradually. We found that using a larger transmit power, P_d may actually decrease compared to a smaller transmit power. Although a higher transmit power can obtain better SNR, the data collection process of sensing nodes is random. It is possible that only a short scan time

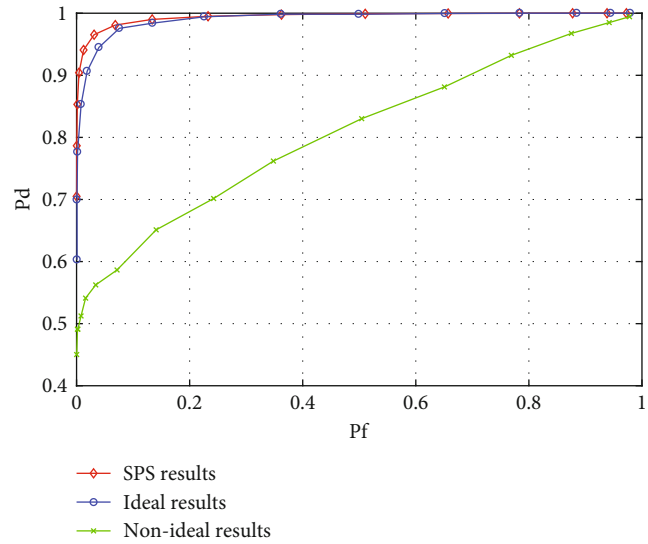

Figure 9: ROC curves of P_d and P_f in different situations.

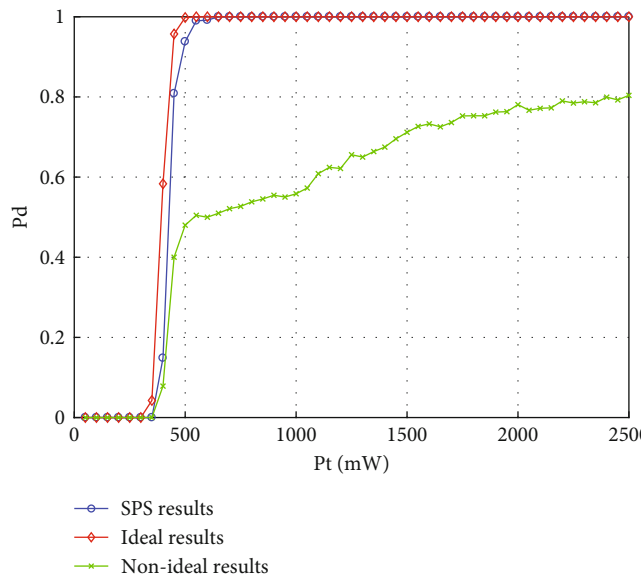

Figure 10: P_d as a function of power in the nonideal situation after using SPS algorithm in the nonideal situation

was acquired at higher transmit powers. In general, using larger transmit power can effectively improve the sensing results.

As shown in the green curve in Figure 11, when the threshold is set to make P_f as 0.01, we discuss the relationship between P_d and the change in the distance of the sensing node from the transmitter. Obviously, it keeps decreasing as the distance increases.

5.3. Sensing Results in Nonideal Situation Based on SPS Algorithm. In this subsection, we consider a more realistic situation. As in Subsection 5.2, the part of the beam scanning process is sampled by the sensing node. The definitions of hyperparameters H_0 and H_1 are the same as those in

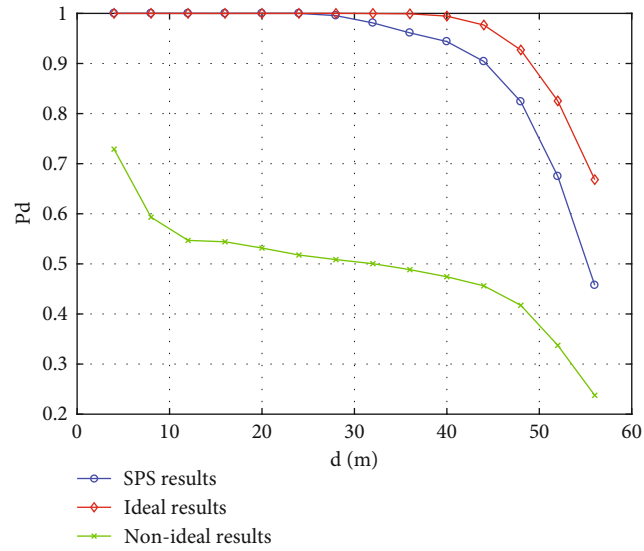

FIGURE 11: P_d as a function of distance in the nonideal situation after using SPS algorithm in the nonideal situation when the sensing node is in the 60° direction of the transmitter

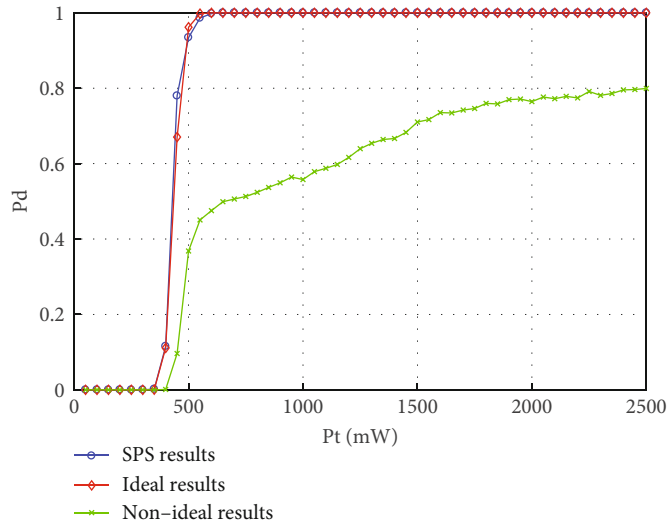

FIGURE 12: P_d as a function of power in the nonideal situation after using SPS algorithm in the nonideal situation when the sensing node is in the 60° direction of the transmitter

Subsection 5.2. When energy detection is implemented, the SPS algorithm is added to optimize the sensing results.

When the beam pattern covers the sensing node, the sensing node can detect a larger signal energy. Our goal is to collect the time period that the beam covers to the sensing node within the sensing period as much as possible. The purpose of adding SPS algorithm is to take the sampling data that the time of beam signal covers the sensing node as the sensing result.

Figure 9 shows the ROC curves of P_d and P_f at different thresholds. The threshold range is the same as the ROC curve in ideal and nonideal situation. In Figure 9, although the sensing node does not sample the whole process of beam scanning, the sensing performance is significantly better than the simulation result without adding the SPS algorithm. The reason is that the sensing result is closer to the situation where the whole process of beam scanning is sampled by sensing nodes, the ideal situation.

The variation of P_d in different transmit powers with setting the threshold to make $P_f$as 0.01 is shown in Figure 10. The blue curve is the relationship between P_d and power after adding the SPS algorithm. The blue curve is the relationship between P_d and power in the ideal situation, and the green curve is in the nonideal situation. After adding the SPS algorithm, the result is much better than that of traditional energy detection without using the SPS algorithm and even approaches the ideal result.

In Figure 11, when the threshold is set to make P_f as 0.01, we discuss the relationship between P_d and the change in the distance of the sensing node from the transmitter. The

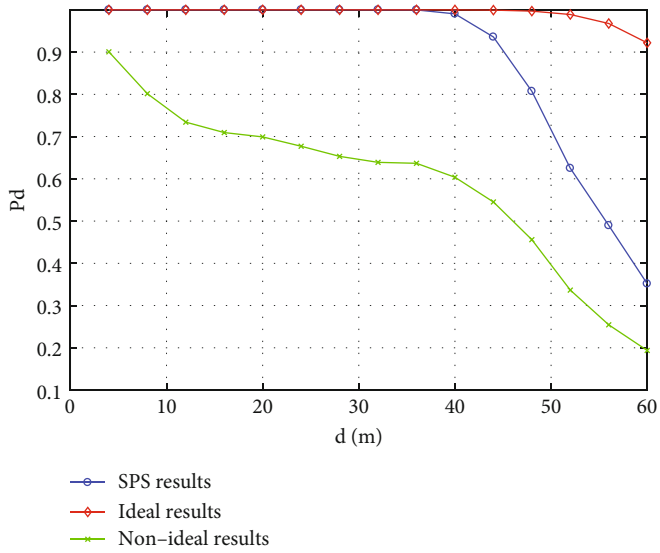

FIGURE 13: P_d as a function of distance in the nonideal situation after using SPS algorithm in the nonideal situation when the sensing node is in the 60° direction of the transmitter

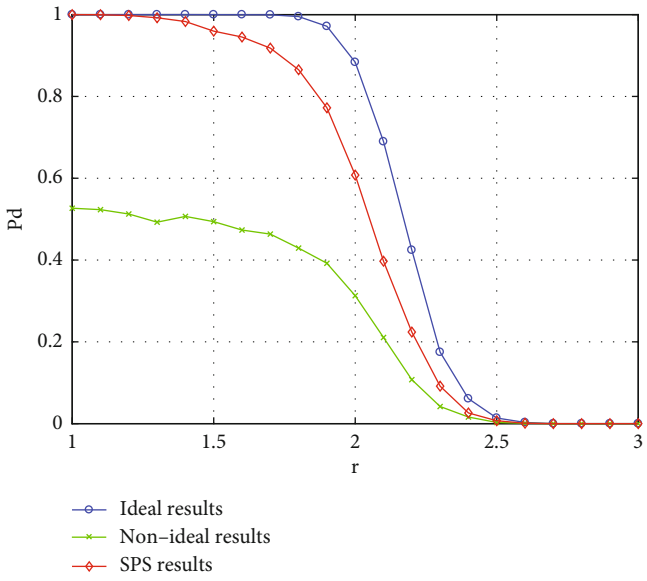

FIGURE 14: P_d as a function of distance sensing period duration

blue curve is the relationship between P_d and the distance between sensing node and transmitter after adding the SPS algorithm. The blue curve is the relationship between P_d and the distance between sensing node and transmitter in the ideal situation, and the green curve is in the nonideal situation. Obviously, when the distance increases to a certain extent, P_d decreases rapidly with the distance continues to increase. After adding the SPS algorithm, the sensing results are significantly better than the experimental results in the nonideal situation and approach the results in the ideal situation.

5.4. Sensing Results of Sensing Nodes in Other Locations. In this subsection, we discuss the sensing performance when the sensing node is in other positions in the ideal situation and nonideal situation and after adding SPS algorithm.

When the sensing node is in other locations, good sensing results can still be obtained after adding SPS algorithm. In Figures 12 and 13, the sensing results when the sensing node is located in the 60° direction of the transmitter are shown, respectively.

The variation of P_d in different transmit powers with setting the threshold to make $P_f$as 0.01 is shown in Figure 12. The blue curve is the relationship between P_d and power after adding the SPS algorithm. After adding SPS algorithm, the sensing result is slightly lower than the ideal red curve and significantly higher than the nonideal green curve. This is consistent with the case where the sensing node is located in the 90° direction of the receiver.

In Figure 13, when the threshold is set to make P_f as 0.01, we discuss the relationship between P_d and the change in the distance of the sensing node from the transmitter. The blue curve is the relationship between P_d and the distance between sensing node and transmitter after adding the SPS algorithm. After adding the SPS algorithm, the sensing result is slightly lower than the ideal red curve and significantly higher than the nonideal green curve. This is consistent with the case where the sensing node is located in the 90° direction of the receiver.

5.5. Setting Time of Sensing Period. The setting of the sensing time needs to be based on the estimation of the scanning period of the multiantenna beam. If the sensing time is set too large, it will result in the acquisition of too much noise.

As shown in Figure 14, where$r$is the ratio of the sensing period to the beam scanning period, we can see that $P_d$keeps decreasing as the sensing period increases. We consider the changes of P_d in the ideal case and nonideal case and after adding the SPS algorithm. In particular, the ideal situation here is defined as that the whole process of beam scanning is within the sensing time. In these three cases, P_d shows a

downward trend, but after adding the SPS algorithm, the performance of P_d is obviously close to the ideal situation.

When the sensing period is too long, there is only noise in most of the time period of sensing, and the time when the beam scans to the sensing node is very small. This results in the scanning signal being covered in long-term noise during the sensing phase.

If the sensing time is set too small, it will be difficult to sample the data that the scanning signal covers the sensing node. In these cases, we can optimize the perception results by using the SPS algorithm. However, if the difference between the sensing time and the beam scanning time is too large, the sensing result will become poor.

6. Conclusion

This paper has studied the issue of spectrum sensing of noncooperative beam signals. For the ideal case, the sensing period is equal to the time of one round of beam scanning and the sensing node collects all the data in the whole process of beam scanning. We use the theoretical derivation method and the Monte Carlo method to verify the performance indicators of spectrum sensing. The results show that in the ideal situation, the spectrum sensing performance indicators verified by the Monte Carlo method are almost consistent with the theoretically derived results and both have good sensing results. For the nonideal situation, that is, the situation closer to the actual situation, we use the traditional energy detection method and the energy detection method after adding the SPS algorithm to verify the performance of spectrum sensing. The experiment uses the Monte Carlo method. The results show that the application of the SPS algorithm in energy detection can effectively improve the performance of spectrum sensing.

Data Availability

Matlab simulation data is available.

Conflicts of Interest

The authors declare that they have no conflicts of interest.

Acknowledgments

This work was supported by the National Key R&D Program of China under Grant 2018YFB1801103 and the National Natural Science Foundation of China (No. 62171462, No. U20B2038, No. 61901520, No. 61931011, and No. 61871398).

References

[1] G. Ding, J. Wang, Q. Wu, Y. D. Yao, F. Song, and T. A. Tsiftsis, "Cellular-base-station-assisted device-to-device communications in TV white space," *IEEE Journal on Selected Areas in Communications*, vol. 34, no. 1, pp. 107–121, 2016.

[2] C. G. Tsinos and K. Berberidis, "Adaptive eigenvalue-based spectrum sensing for multi-antenna cognitive radio systems," *IEEE Transactions on Wireless Communications*, vol. 14, no. 3, pp. 1703–1715, 2013.

[3] J. L. Wang, G. Ding, Q. Wu, L. Shen, and F. Song, "Spatial-temporal spectrum hole discovery: a hybrid spectrum sensing and geolocation database framework," *Chinese Science Bulletin*, vol. 59, no. 16, pp. 1896–1902, 2014.

[4] H. Zhang and C. Guo, "Beam alignment-based mmWave spectrum sensing in cognitive vehicular networks," in *2019 IEEE Global Conference on Signal and Information Processing (GlobalSIP)*, pp. 1–5, Ottawa, ON, Canada, 2019.

[5] R. Rytel-Andrianik, "Efficient matched filtering and beamforming for coherent MIMO radar," in *2016 IEEE International Symposium on Phased Array Systems and Technology (PAST)*, pp. 1–6, Waltham, MA, USA, 2016.

[6] V. Prithiviraj, B. Sarankumar, A. Kalaiyarasan, P. P. Chandru, and N. N. Singh, "Cyclostationary analysis method of spectrum sensing for cognitive radio," in *2011 2nd International Conference on Wireless Communication, Vehicular Technology, Information Theory and Aerospace & Electronic Systems Technology (Wireless VITAE)*, pp. 1–5, Chennai, India, 2011.

[7] H. Kim, K. Granström, L. Gao, G. Battistelli, S. Kim, and H. Wymeersch, "5G mmWave cooperative positioning and mapping using multi-model PHD filter and map fusion," *IEEE Transactions on Wireless Communications*, vol. 19, no. 6, pp. 3782–3795, 2020.

[8] W. Lu, P. Si, G. Huang et al., "SWIPT cooperative spectrum sharing for 6G-enabled cognitive IoT network," *IEEE Internet of Things Journal*, vol. 8, no. 20, pp. 15070–15080, 2021.

[9] K. C. Ho and S. H. Tsai, "A novel multiuser beamforming system with reduced complexity and beam optimizations," *IEEE Transactions on Wireless Communications*, vol. 18, no. 9, pp. 4544–4557, 2019.

[10] F. Shen, G. Ding, Z. Wang, and Q. Wu, "UAV-based 3D Spectrum sensing in Spectrum-heterogeneous networks," *IEEE Transactions on Vehicular Technology*, vol. 68, no. 6, pp. 5711–5722, 2019.

[11] C. Liu, *Spatial Spectrum Based Spectrum Sensing in Cognitive Radio*, 2017.

[12] Y. H. Chen and Z. P. Shi, "A method of multi-antenna spatial spectrum sensing based on noncircular signals," in *2020 IEEE 20th International Conference on Communication Technology (ICCT)*, pp. 863–866, Nanning, China, 2020.

[13] A. Alizadeh, H. R. Bahrami, M. Maleki, and S. Sastry, "Spatial sensing and cognitive radio communication in the presence of a *K*-user interference primary network," *IEEE Journal on Selected Areas in Communications*, vol. 33, no. 5, pp. 741–754, 2015.

[14] T. Wilcoxd, A. Kortun, T. Ratnarajah, C. B. Papadias, and M. Sellathurai, "On spatial domain cognitive radio using single-radio parasitic antenna arrays," *IEEE Journal on Selected Areas in Communications*, vol. 31, no. 3, pp. 571–580, 2013.

[15] Y. Y. Wang, J. T. Chen, and W. H. Fang, "TST-MUSIC for joint DOA-delay estimation," *IEEE Transactions on Signal Processing*, vol. 49, no. 4, pp. 721–729, 2001.

[16] J. M. Kim, O. K. Lee, and J. C. Ye, "Compressive MUSIC: revisiting the link between compressive sensing and array signal processing," *IEEE Transactions on Information Theory*, vol. 58, no. 1, pp. 278–301, 2012.

[17] P. Vallet, X. Mestre, and P. Loubaton, "Performance analysis of an improved MUSIC DOA estimator," *IEEE Transactions on Signal Processing*, vol. 63, no. 23, pp. 6407–6422, 2015.

[18] J. Xie, Z. Fu, and H. Xian, "Spectrum sensing based on estimation of direction of arrival," in *International Conference on Computational Problem-Solving*, pp. 39–42, Li Jiang, China, 2010.

[19] R. Zhang, T. Lim, Y. C. Liang, and Y. Zeng, "Multi-antenna based spectrum sensing for cognitive radios: a GLRT approach," *IEEE Transactions on Communications*, vol. 58, no. 1, pp. 84–88, 2010.

[20] S. Lee, I. Nam, and D. Kim, "Electrical Beam Scan Antenna Using Miniaturized Frequency Selective Reflectors," *In 2018 International Symposium on Antennas and Propagation (ISAP)*, pp. 1-2, 2018.

[21] Q. Zeng, Z. Xue, W. Ren, and W. Li, "Dual-band beam-scanning antenna using rotatable planar phase gradient transmitarrays," *IEEE Transactions on Antennas and Propagation*, vol. 68, no. 6, pp. 5021–5026, 2020.

[22] C. X. Mao, S. Gao, and Y. Wang, "Broadband high-gain beam-scanning antenna array for millimeter-wave applications," *IEEE Transactions on Antennas and Propagation*, vol. 65, no. 9, pp. 4864–4868, 2017.

[23] D. Cabric, S. M. Mishra, and R. W. Brodersen, "Implementation issues in spectrum sensing for cognitive radios," in *Conference Record of the Thirty-Eighth Asilomar Conference on Signals, Systems and Computers*, pp. 772–776, Pacific Grove, CA, USA, 2004.

[24] J. Wildman, P. Nardelli, M. Latva-Aho, and S. Weber, "On the joint impact of beamwidth and orientation error on throughput in directional wireless Poisson networks," *IEEE Transactions on Wireless Communications*, vol. 13, no. 12, pp. 7072–7085, 2014.

[25] H. L. Van Trees, *Detection, Estimation, and Modulation Theory, Optimum Array Processing (Part IV), [M.S. thesis]*, John Wiley and Sons, Inc, New York, 2002.

[26] H. Urkowitz, "Energy detection of unknown deterministic signals," *Proceedings of the IEEE*, vol. 55, no. 4, pp. 523–531, 1967.

[27] F. F. Digham, M. S. Alouini, and M. K. Simon, "On the energy detection of unknown signals over fading channels," *IEEE Transactions on Communications*, vol. 55, no. 1, pp. 21–24, 2007.

[28] J. Gao, X. Yi, C. Zhong, X. Chen, and Z. Zhang, "Deep learning for spectrum sensing," *IEEE Wireless Communications Letters*, vol. 8, no. 6, pp. 1727–1730, 2019.